Journal of Magnetism and Magnetic Materials 591 (2024) 171683

Contents lists available at ScienceDirect

Journal of Magnetism and Magnetic Materials

journal homepage: www.elsevier.com/locate/jmmm

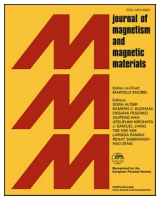

Research article

High-field magnetoresistance measurements on $Ni_{75}Co_{25}$ and $Ni_{40}Co_{60}$ alloys at 3 K and 300 K

I. Bakonyi [a,*], F.D. Czeschka [b,1], V.A. Isnaini [a,2], A.T. Krupp [b], J. Gubicza [c], L.K. Varga [a], L. Péter [a]

[a] Institute for Solid State Physics and Optics, HUN-REN Wigner Research Centre for Physics, H–1121 Budapest, Konkoly-Thege út 29-33, Hungary
[b] Walther-Meißner-Institute for Low Temperature Research, Bavarian Academy of Sciences and Humanities. Walther-Meißner-Straße 8, D-85748 Garching, Germany
[c] Department of Materials Physics, Eötvös Loránd University, H-1117 Budapest, Pázmány Péter sétány 1/A, Hungary

ARTICLE INFO

Keywords:
Anisotropic magnetoresistance
Ni-Co alloys

ABSTRACT

In the present work, a detailed field dependence of the resistivity of $Ni_{75}Co_{25}$ and $Ni_{40}Co_{60}$ bulk alloys was measured at $T = 3$ K and 300 K up to high magnetic fields. The focus of the study was to determine the anisotropic magnetoresistance (AMR) and to get a quantitative description of the field-induced resistivity change, the latter not yet being available for Ni-Co alloys. The AMR parameters were derived from the resistivity data in the magnetically saturated (monodomain) state by using the Kohler analysis. The values of the AMR ratio were found to be close to the relevant previous data both at low and high temperatures. Due to the measurement precision and careful data evaluation, our AMR data obtained on well-characterized samples can be considered as reference values for the bulk state of the investigated compositions. In addition, also the resistivity anisotropy splitting was determined. The experimentally found field dependence of the resistivity at both $T = 3$ K and 300 K turned out to be at variance with the current theoretical descriptions both for the resistivity increase due to the ordinary magnetoresistance effect being significant at $T = 3$ K and for the resistivity decrease due to the magnon suppression process at $T = 300$ K, invoking for a refinement of theory in both cases.

1. Introduction

The ferromagnetic elements Fe, Co and Ni as well as their mutual alloys play an important role in the field of spintronics since the electrodes in spintronic devices are mostly composed of these metals and alloys [1] and they are also widely used in various magnetoresistive sensors [2]. It is, therefore, an important task to improve our knowledge about their magnetic, electrical transport and magnetotransport properties. Particularly interesting is their anisotropic magnetoresistance (AMR) behavior [3–6], especially because recently there have been attempts to separate the AMR into intrinsic and extrinsic contributions (see, e.g., Ref. [7]).

Along this line, we have devoted efforts in recent years to studying the AMR of well-characterized samples of the ferromagnetic metals Ni and Co. We have reported on the room-temperature AMR of bulk (well-annealed, coarse grained) and nanocrystalline (nc) samples of Ni metal [8]. Furthermore, it could be shown in a room-temperature study [9] on polycrystalline Co samples with fully hexagonal close-packed (hcp) structure and with predominantly face-centered cubic (fcc) structure that the AMR ratio of fcc-Co is larger by nearly a factor of 2 than that of hcp-Co.

We have also studied the magnetoresistance (MR) of a bulk and a nc Ni sample up to high magnetic fields at 3 K and 300 K [10]. The accurate measurement of the resistivity over a broad range of magnetic field H enabled an evaluation of the MR(H) curves on the basis of the so-called Kohler plot [11]. With the help of the Kohler plots, the AMR parameters such as the resistivity anisotropy splitting ($\Delta\rho_{AMR}$) [8,10,12] and the AMR ratio can be straightforwardly derived.

According to Kohler's rule [11], the magnetic-field-induced relative resistivity change $\Delta\rho(H)/\rho_o = [\rho(H) - \rho_o]/\rho_o$ is a function of the ratio H/ρ_o only where $\rho(H)$ is the resistivity ρ in a magnetic field H and ρ_o is the resistivity measured in the absence of a magnetic field. This can be formulated as $\Delta\rho(H)/\rho_o = F(H/\rho_o)$ where the Kohler function F is to be determined empirically from the measured MR(H) data since F cannot be derived theoretically.

The validity of Kohler's rule has been demonstrated experimentally

* Corresponding author.
E-mail address: bakonyi.imre@wigner.hun-ren.hu (I. Bakonyi).
[1] Present address: BSH Hausgeräte GmbH, Munich, Germany.
[2] Present address: UIN Sulthan Thaha Saifuddin, Jambi, Indonesia.

https://doi.org/10.1016/j.jmmm.2023.171683
Received 21 October 2023; Received in revised form 17 December 2023; Accepted 26 December 2023
Available online 29 December 2023
0304-8853/© 2023 The Author(s). Published by Elsevier B.V. This is an open access article under the CC BY-NC-ND license (http://creativecommons.org/licenses/by-nc-nd/4.0/).

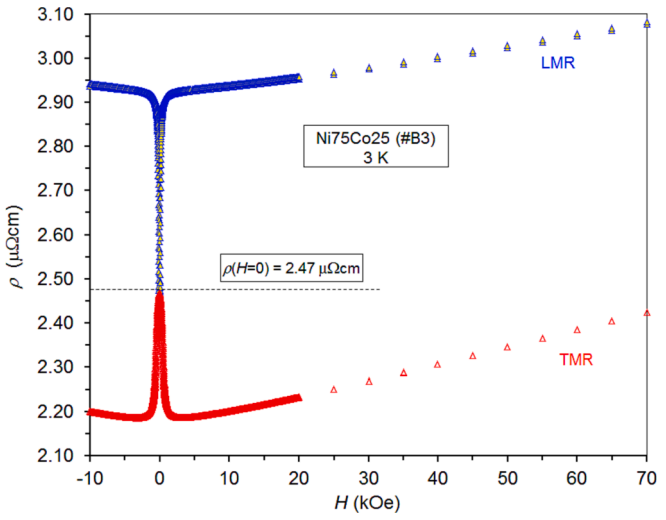

Fig. 1. Field dependence of the resistivity ρ at $T = 3$ K for the $Ni_{75}Co_{25}$ alloy with magnetic field orientations as indicated (LMR, TMR) in the magnetic field range from −10 kOe to + 70 kOe.

for most normal (non-magnetic) metals [11,13]. This means that the MR (H) data from samples with different residual resistivities (due to different concentration of chemical impurities or lattice defects) of a given metal fall on a single curve when displaying the data in the form of a Kohler plot: $\Delta\rho(H)/\rho_o$ vs H/ρ_o. Schwerer and Silcox [14] recognized that in ferromagnets, instead of the magnetic field H, the magnetic induction $B = H + 4\pi M_s$ should be used in Kohler's rule where M_s is the saturation magnetization of the ferromagnet. The rationale behind this is the fact that, in a ferromagnet, not the externally applied magnetic field H, but the magnetic induction B is the effective field acting on the electron trajectories [5,6]. It is noted that, for a correct treatment, the demagnetizing field should also be taken into account in the expression of B [5,12]. In our strip-shaped foil geometry [12], the demagnetizing field can be usually neglected besides the other terms for magnetic fields applied in the plane of the thin strip sample (i.e., the expression $B = H + 4\pi M_s$ is approximately valid in most cases); it should be properly considered, however, for the case of an out-of-plane magnetic field [5,12].

The magnetoresistance characteristics of Ni-Co alloys have been intensively investigated in the past as summarized in Ref. 15 where a comparison with available theoretical AMR parameters was also made. In previous works, the emphasis was mainly on determining the AMR ratio. In the present work, MR(H) measurements were performed at $T =$ 3 K and 300 K up to high magnetic fields on two Ni-Co alloys in order to establish quantitatively the field dependence of the resistivity not available beforehand. The first alloy composition chosen was $Ni_{75}Co_{25}$ which has the highest AMR ratio in the Ni-Co system and the second one was $Ni_{40}Co_{60}$ which is close to the borderline of the existence of face-centred cubic (fcc) phase in this alloy system. The MR(H) measurements were carried out for both alloys up to $H = 70$ kOe with the magnetic field oriented in the plane of the alloy foils, whereas for the $Ni_{75}Co_{25}$ alloy, MR(H) measurements were also performed at both temperatures up to $H = 140$ kOe with the magnetic field oriented perpendicular to the foil plane. The measured MR(H) curves were evaluated in each case with the Kohler plots, similarly to the procedure applied for Ni metal in Ref. 10.

The paper is organized as follows. In Section 2, the investigated Ni-Co alloy samples, the electronic transport measurement configurations in a magnetic field and the measurement technique for the magnetoresistance will be presented. The experimental results for the magnetoresistance data of the $Ni_{75}Co_{25}$ and $Ni_{40}Co_{60}$ alloy samples studied with in-plane magnetic fields up to $H = 70$ kOe are presented separately for $T =$ 3 K in Section 3 and for $T = 300$ K in Section 4. These sections also include a comparison of the results for the two alloys at each temperature as well as with previously reported experimental results on a nc-Ni sample [10]. The MR(H) measurements on the $Ni_{75}Co_{25}$ alloy in out-of-plane magnetic fields will be presented in Section 5. A summary of the present results will be given in Section 6.

2. Experimental

2.1. Samples investigated: preparation, microstructure and zero-field resistivity

The results of electrical transport measurements to be presented here were obtained on thin Ni-Co alloy foil samples. By melting electrolytic grade Ni with 0.6 at.% Fe nominal (maximum) impurity content and electrolytic grade Co with 0.5 at.% Fe and 0.2 at.% Ni nominal (maximum) impurity content, ingot alloys were prepared for the compositions $Ni_{75}Co_{25}$ (sample #B3) and $Ni_{40}Co_{60}$ (sample #B4). A cold-rolling process was applied in several steps down to a thickness of 55 μm ($Ni_{75}Co_{25}$) and 66 μm ($Ni_{40}Co_{60}$). The foils were subjected to a heat treatment at about 700 °C for 1 h in a protecting hydrogen atmosphere to release the stresses introduced by the cold-rolling procedure.

Chemical analysis was carried out by energy-dispersive X-ray (EDX) spectroscopy in a TESCAN MIRA3 scanning electron microscope equipped with an EDAX Element analyzer. The EDS analysis was performed with 20 kV acceleration voltage, and the K lines of the iron group metals were used for assessing the composition. For each alloy, EDX measurements were carried on four spots each having a typical area of 0.1 mm^2. The measured Ni and Co concentrations agreed with the nominal values within about 0.5 at.% for both alloys, and for a given alloy, the measured four values revealed an inhomogeneity of not more than about 0.3 at.%. Although the electrolytic grade Ni and Co starting metals were specified as having a relatively large Fe impurity allowance (see above), the actual Fe content was found to be definitely not more than 0.05 at.% according to the EDX analysis. Besides a small amount of C and O probably in the form of surface contamination, no other non-metallic impurities could be found within the usual EDS detection limit of about 0.1 at.%.

The phase composition of the Ni-Co samples was studied by a standard X-ray diffraction (XRD) technique using CuK_α radiation (wavelength: 0.15418 nm). The observed Bragg peaks in the measured XRD patterns could be identified with a face-centered cubic (fcc) structure for both investigated samples and, thus, no hexagonal close-packed (hcp) phase was present even for the higher Co content. The XRD peak width of the Ni-Co alloys was typically as narrow as the instrumental broadening. According to former investigations [16], such narrow diffraction peaks usually indicate crystallite sizes larger than one micrometer. This crystallite size is typical for well-annealed metals and, therefore, the above-described Ni-Co alloy samples can be considered as representing the bulk state of these alloys.

The room-temperature zero-field resistivity (ρ_o) data of the two Ni-Co alloys were measured by the method described in Ref. 17. This method is based on determining the effective strip width by imaging the strip surface and calculating the foil thickness from the measured strip mass and by using the density of the alloy. By measuring the resistivity of pure Ni foil samples, the accuracy of this resistivity measurement method was shown to be ± 3 % [17]. Since the density of Ni and Co differ by 0.1 % only [18] which is much less than the overall resistivity error, we used 8.90 g/cm^3 for the density of both Ni-Co alloys. In this manner, we obtained $\rho_o(300\ K) = 10.66 \pm 0.32$ μΩcm for the $Ni_{75}Co_{25}$ alloy (sample #B3) and $\rho_o(300\ K) = 8.47 \pm 0.25$ μΩcm for the $Ni_{40}Co_{60}$ alloy (sample #B4). These values match well the data collected for the room-temperature resistivity of Ni-Co alloys [15].

In the present work, we obtained the low-temperature zero-field resistivity $\rho_o(3\ K) = 2.47$ μΩcm for the $Ni_{75}Co_{25}$ alloy and $\rho_o(3\ K) =$ 1.78 μΩcm for the $Ni_{40}Co_{60}$ alloy which values actually correspond to

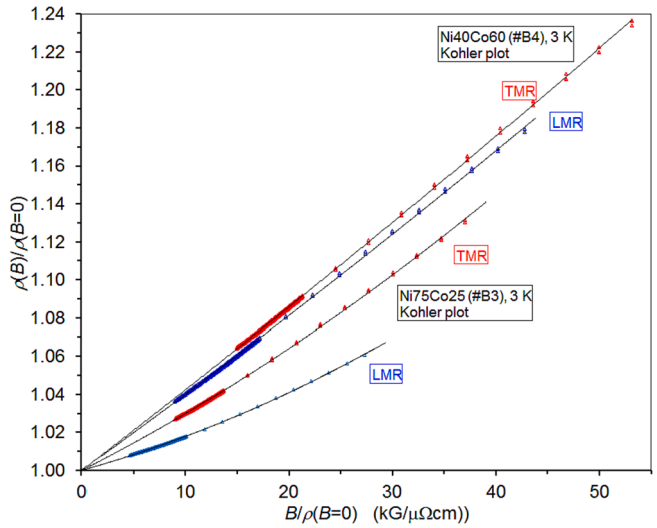

Fig. 2. Kohler plot $\rho(B)/\rho(B{=}0)$ vs $B/\rho(B{=}0)$ of the MR(H) data at $T = 3$ K for the $Ni_{75}Co_{25}$ and $Ni_{40}Co_{60}$ alloys with magnetic field orientations as indicated (LMR, TMR). The experimental data are the symbols (triangles), the solid lines are the second-order polynomial fitting functions providing an empirical analytical form of the Kohler function F (the fit parameters are given in the Appendix).

the residual resistivity of the two alloys. From these data, we get for the residual resistivity ratio RRR = $\rho_o(300K)/\rho_o(3K)$ the values 4.32 for the $Ni_{75}Co_{25}$ alloy and 4.76 for the $Ni_{40}Co_{60}$ alloy.

2.2. Magnetoresistance measurements

The measurement of the resistivity was performed with a four-point probe on rectangular strips about 1 mm wide and about 5 mm long cut from the alloy foils with the current flowing along the length of the strip and by cycling the magnetic field H between the positive and negative maximum values. First, the MR(H) curves were measured for both alloys with the magnetic field in the strip plane and oriented either parallel (longitudinal MR = LMR) or perpendicular (transverse MR = TMR) to the current flow. Second, for the $Ni_{75}Co_{25}$ alloy the resistivity was also measured with the magnetic field oriented perpendicular to the strip plane (this is called polar magnetoresistance (PMR) measurement). For more details of contacting the strips and measuring the resistance, see Ref. 10.

3. Magnetoresistance results with in-plane magnetic fields at $T = 3$ K for $Ni_{75}Co_{25}$ and $Ni_{40}Co_{60}$

Fig. 1 shows the field dependence of the resistivity for the $Ni_{75}Co_{25}$ alloy at $T = 3$ K in the LMR and TMR configurations. The overall behavior is typical for a metallic ferromagnet at low temperatures with a sizeable residual resistivity [10,12]. This means that at low magnetic fields the characteristic AMR feature is seen (LMR > 0, TMR < 0) whereas for magnetic fields beyond magnetic saturation, a monotonic, non-saturating increase of both components occurs, arising from the non-negligible ordinary magnetoresistance (OMR) [4–6,10,12]. The $Ni_{40}Co_{60}$ alloy has qualitatively very similar characteristics, only the magnitude of the resistivity and the rate of change of the resistivity with magnetic field are different.

It can be seen that the resistivity variation with magnetic field is very rapid at low magnetic fields for both measurement configurations and reflects the magnetization process of ferromagnets from the demagnetized state to the saturation of the magnetization as explained by Bozorth [3] on the basis of the ferromagnetic domain picture. The MR (H) curves in the low-field region (not shown) reveal a hysteresis behavior as usually observed also in the low-field magnetization curves $M(H)$. Nevertheless, the main conclusions of the present paper about the AMR parameters to be shown later are not influenced by the low-field features of the magnetoresistance curves since these parameters are determined from the data in the magnetically saturated high-field region only.

Above the saturation fields which are approximately around the breaks in the MR(H) curves, the resistivity variation is much weaker, and it shows a modest monotonous increase with similar rates for both MR configurations of each alloy.

We will analyze the data on the basis of the Kohler plots by taking into account that the magnetic field H should be replaced with the magnetic induction $B = H + 4\pi M_s$ (at $T = 3$ K, we have $4\pi M_s = 9.35$ kG for $Ni_{75}Co_{25}$ and $4\pi M_s = 13.466$ kG for $Ni_{40}Co_{60}$). Accordingly, Kohler's rule for a ferromagnet will take the form $\Delta\rho(B)/\rho(B=0) = [\rho(B) - \rho(B=0)]/\rho(B=0) = F[B/\rho(B=0)]$ where we have now replaced the zero-field resistivity $\rho_o = \rho(H=0)$ with $\rho(B=0)$ to emphasize that the resistivity at zero induction is the normalizing factor for ferromagnets. Kohler's rule can be transformed also into the following form: $\rho(B)/\rho(B=0) = 1 + F[B/\rho(B=0)]$ [10,14]. This implies that if we display $\rho(B)/\rho(B=0)$ as a function of $B/\rho(B=0)$ which is the Kohler plot, then the Kohler function $F[B/\rho(B=0)]$ should extrapolate to 1 when $B \to 0$.

For performing the data analysis with the Kohler plot similarly as was done for pure Ni [10], we should get a first estimate for the value of the experimentally unattainable zero-induction resistivity $\rho(B = 0)$ for both the LMR and TMR components. For this purpose, we displayed the measured resistivity data $\rho(B)$ against the magnetic induction B for both alloys and fitted the experimental MR(H) data with a polynomial with freely variable $\rho(B = 0)$ value. It was found for the current data that a second-order polynomial is sufficient since going to higher orders, the normalized fit quality parameter (R^2) given by the square of the Pearson product moment correlation coefficient improved only insignificantly. The fit quality was found to be very good ($R^2 > 0.999$ in each case) and, also, no systematic deviation between the experimental data and the fitted curves could be observed.

For constructing the Kohler plots for the LMR and TMR components, i.e., displaying the $\rho(B)/\rho(B = 0)$ data as a function of $B/\rho(B = 0)$, we take first the $\rho_L(B = 0)$ and $\rho_T(B = 0)$ values equal to those obtained from the $\rho(B)$ vs B plots. The resulting Kohler plots for the LMR(H) and TMR (H) data measured at $T = 3$ K are shown for both alloys in Fig. 2. Since the form of the Kohler function F is not known, we fit the data again with an empirical polynomial function by using the constraint that the Kohler function $F[B/\rho(B = 0)]$ should extrapolate to 1 when $B \to 0$. As found for the $\rho(B)$ vs B data above, it turned out that a second-order polynomial could give an excellent fit to the current data. By finely tuning the value of $\rho(B = 0)$, it was established that the same zero-induction resistivity values with the same fit quality provide the best fit to the Kohler plot data as obtained for the $\rho(B)$ vs B plots. Evidently, data in the magnetically saturated state ($H \geq 4$ kOe for LMR and $H \geq 10$ kOe for TMR) should only be taken into account in the Kohler plot analysis.

As a result of the fitting procedure, we have now the zero-induction resistivities $\rho_L(B = 0)$ and $\rho_T(B = 0)$ of both alloys at $T = 300$ K which values are summarized in Table 1. By introducing the notations [10,12] $\rho_L(B = 0) = \rho_{Ls}$ and $\rho_T(B = 0) = \rho_{Ts}$ where the superscript s refers to the fact that the zero-induction resistivities are obtained from the MR(H) data in the magnetically saturated state, one can then derive the isotropic resistivity $\rho_{is} = (1/3)\,\rho_{Ls} + (2/3)\,\rho_{Ts}$, the resistivity anisotropy splitting $\Delta\rho_{AMR} = \rho_{Ls} - \rho_{Ts}$ and the AMR ratio = $\Delta\rho_{AMR}/\rho_{is}$ [10,12] which values are also given in Table 1. The AMR ratio at $T = 3$ K for the $Ni_{75}Co_{25}$ alloy matches well the reported low-temperature values whereas for the $Ni_{40}Co_{60}$ alloy, our value is definitely larger than the reported values, the latter ones all falling below 20 % [15].

According to the previous discussions, the variation of the resistivity with magnetic induction in the magnetically saturated (monodomain) state could be properly described for the measured data by an empirical second-order polynomial fitting function $\rho(B) = \rho(B = 0) + \alpha \cdot B + \beta \cdot B^2$

Table 1
Parameters characterizing the field dependence of the induced resistivity change $\Delta\rho(B) = \rho(B) - \rho(B = 0)$ of the $Ni_{75}Co_{25}$ and $Ni_{40}Co_{60}$ alloys at $T = 3$ K for the LMR and TMR configurations. The parameter values were obtained from fits of the experimental data in the magnetically saturated region to the function $\Delta\rho(B) = \alpha \cdot B + \beta \cdot B^2$ with $\rho(B = 0)$ values obtained from the Kohler plot analysis. The last three columns provide the isotropic resistivity and the AMR parameters for the two alloys as deduced from the Kohler plots.

$T = 3$ K fitted parameters		$\rho(B = 0)$ (μΩ·cm)	α (μΩ·cm/kG)	β (μΩ·cm/(kG)^2)	ρ_{is} (μΩ·cm)	AMR parameters $\Delta\rho_{AMR}$ (μΩ·cm)	AMR ratio (%)
$Ni_{75}Co_{25}$ (#B3)	LMR	2.91	$+1.40 \cdot 10^{-3}$	$+10.47 \cdot 10^{-6}$	2.40	0.767	32.0
	TMR	2.14	$+2.84 \cdot 10^{-3}$	$+9.24 \cdot 10^{-6}$			
$Ni_{40}Co_{60}$ (#B4)	LMR	1.95	$+3.93 \cdot 10^{-3}$	$+3.66 \cdot 10^{-6}$	1.70	0.380	22.4
	TMR	1.57	$+4.19 \cdot 10^{-3}$	$+3.21 \cdot 10^{-6}$			

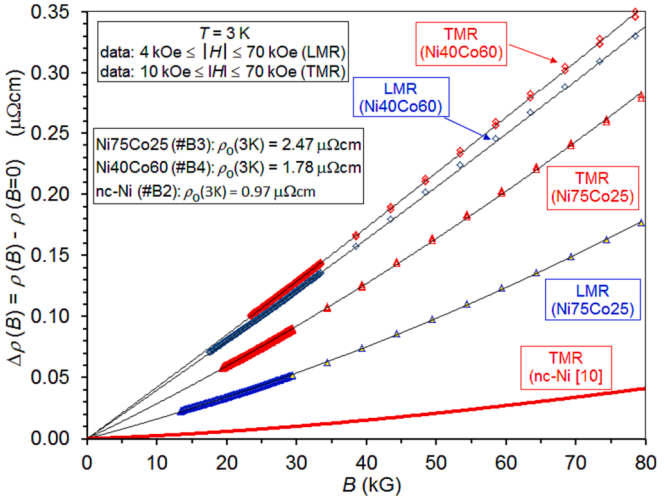

Fig. 3. Resistivity change $\Delta\rho(B) = \rho(B) - \rho(B = 0)$ vs B in the magnetically saturated state at T = 3 K for the $Ni_{75}Co_{25}$ and $Ni_{40}Co_{60}$ alloys. The experimental data are the symbols (triangles and diamonds), the solid lines are the corresponding second-order polynomial fitting functions. The reference resistivity was the zero-induction resistivity $\rho(B = 0)$ determined for the given measurement configuration (LMR and TMR) from a Kohler plot analysis. For comparison, the thick (red) line represents the TMR data obtained on a nc–Ni foil [10]. (For interpretation of the references to colour in this figure legend, the reader is referred to the web version of this article.)

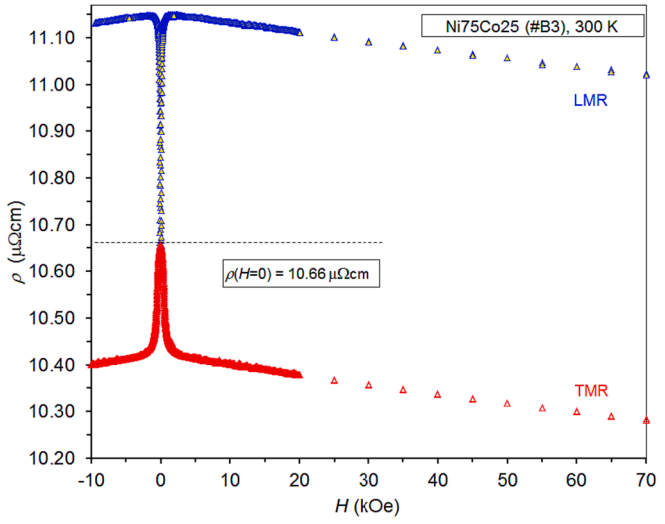

Fig. 4. Field dependence of the resistivity ρ at $T = 300$ K for the $Ni_{75}Co_{25}$ alloy with magnetic field orientations as indicated (LMR, TMR) in the magnetic field range from −10 kOe to + 70 kOe.

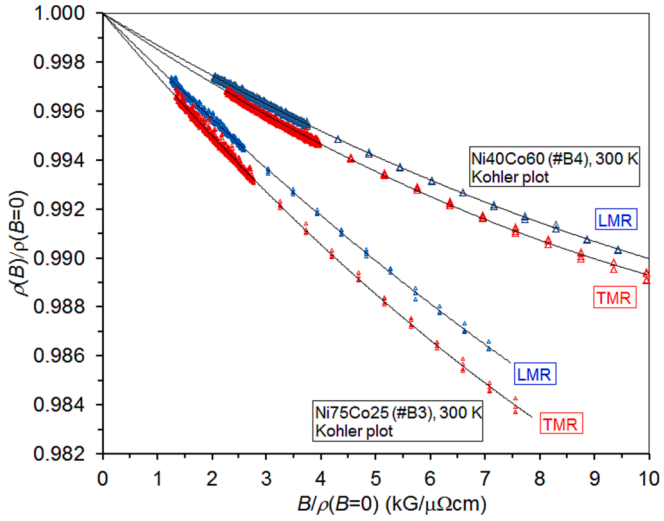

Fig. 5. Kohler plot $\rho(B)/\rho(B{=}0)$ vs $B/\rho(B{=}0)$ at $T = 300$ K for the $Ni_{75}Co_{25}$ and $Ni_{40}Co_{60}$ alloys with magnetic field orientations as indicated (LMR, TMR) for the MR(H) data in the magnetic field range 5 kOe ≤ $|H|$ ≤ 70 kOe. The experimental data are the symbols (triangles), the solid lines are the second-order polynomial fitting functions providing an empirical analytical form of the Kohler function F (the fit parameters are given in the Appendix).

for both alloys. In order to better compare the two Ni-Co alloys, the induced resistivity change $\Delta\rho(B) = \rho(B) - \rho(B = 0) = \alpha \cdot B + \beta \cdot B^2$ is displayed in Fig. 3 as a function of the magnetic induction B for both samples. This means that for each component (LMR and TMR), the resistivity change $\Delta\rho(B)$ is referred to its zero-induction value. The fit parameters α·and β· are also specified in Table 1.

Both samples exhibit a resistivity increase of comparable magnitude and this increase can be attributed to the OMR contribution due to the Lorentz force acting on the conduction electrons [5,6]. For both Ni-Co alloys, the TMR component is larger than the LMR one and this behavior was previously explained for the similar results obtained on pure Ni metal [10]. The magnitude of the OMR effect is somewhat larger for $Ni_{40}Co_{60}$ than for $Ni_{75}Co_{25}$ which may be due to the smaller zero-field resistivity of the former alloy. The smaller resistivity corresponds to a longer electron mean free path and, therefore, the Lorentz force can induce stronger rotation of the electron paths, leading finally to a larger resistivity increase for the $Ni_{40}Co_{60}$ alloy. In agreement with the fit parameters in Table 1, one can see in Fig. 3 that the curvature is stronger for the data of the $Ni_{75}Co_{25}$ alloy with the origin of this difference being unclear. This is rather strange as this alloy has the smaller Lorentz-force contribution.

In Fig. 3, previous results on the TMR component of a nc-Ni metal [10] are also displayed. The basic behavior is the same as for the two Ni-Co alloys studied here although the nc-Ni sample seems to have a smaller

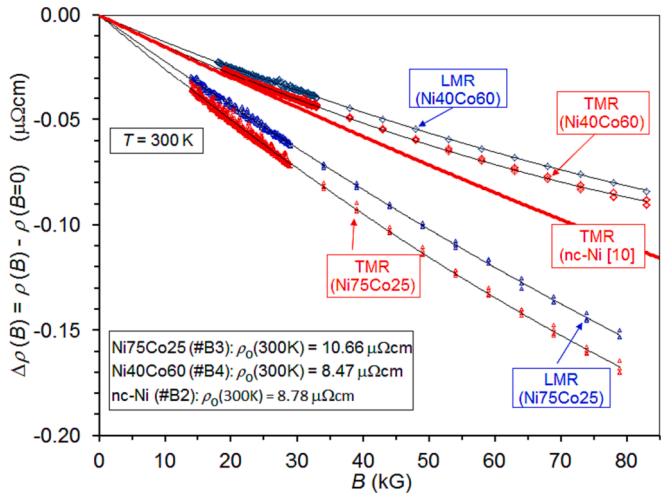

Fig. 6. Resistivity change $\Delta\rho(B) = \rho(B) - \rho(B = 0)$ vs B in the magnetically saturated state at T = 300 K for the $Ni_{75}Co_{25}$ and $Ni_{40}Co_{60}$ alloys. The experimental data are the symbols (triangles and diamonds), the solid lines are the corresponding second-order polynomial fitting functions. The reference resistivity in each case was the zero-induction resistivity $\rho(B = 0)$ determined for the given measurement configuration (LMR and TMR) from a Kohler plot analysis. For comparison, the thick (red) line represents the TMR data obtained on a nc–Ni foil [10]. (For interpretation of the references to colour in this figure legend, the reader is referred to the web version of this article.)

field-induced resistivity change. By considering that the zero-field resistivity of the nc-Ni metal [10] is about half of that of the $Ni_{75}Co_{25}$ alloy and, therefore, its electron mean free path is about twice larger, this result is rather surprising. A possible explanation for the difference in the magnitude of the OMR terms between nc-Ni metal and the Ni-Co alloys may lie in the difference of the origin of the finite (non-zero) residual resistivities.

Namely, the residual resistivity of the Ni-Co alloys arises from the atomic-scale chemical disorder of the alloy. On the other hand, in nc-Ni the residual resistivity arises from the presence of a large density of grain boundaries which represent strong scattering features and are also present throughout the whole sample volume uniformly. However, the latter are distributed not on an atomic scale but rather on the scale of the typical grain size which is for this particular nc-Ni sample is about 100 nm [10]. According to the theoretical calculations of Gall [19], for Ni metal we have $\rho_o\lambda = 4.07{\cdot}10^{-16}$ Ωm^2 where λ is the electron mean free path from which we get λ(nc-Ni;3K) = 42 nm with our measured ρ_o(nc–Ni;3K) = 0.97 μΩcm value [10]. Unfortunately, for alloys there are no direct data either for the product $\rho_o\lambda$ or for λ itself, at most we may guess that for the two investigated Ni-Co alloys λ is certainly smaller than the value for the nc-Ni sample, simply due to their larger zero-field resistivities (see Fig. 3).

In view of these results, at a given temperature the Lorentz-field-induced resistivity contribution may not only depend on the electron mean free path which scales inversely with the sample resistivity, but also on the length scale of the occurrence of the electron scattering centers.

We should make a note here on the field dependence of the ordinary magnetoresistance arising due to the Lorentz force acting on the electron trajectories. The field dependence of the resistivity increase due to the OMR effect is usually assumed to scale with the square of the magnetic induction [4–6]. However, the above presented accurate experimental data on the two Ni-Co alloys and also previously reported similar results on a nc-Ni foil [10] demonstrate that at low temperatures where the Lorentz-force-induced electron path modifications could effectively contribute to the resistivity change, the observed field dependence of the resistivity always contains a linear term as well. It requires further theoretical efforts to clarify if the OMR term can indeed include a linear term as well or, if not, what is the origin of the definitely non-negligible linear term.

4. Magnetoresistance properties with in-plane magnetic fields at $T = 300$ K for $Ni_{75}Co_{25}$ and $Ni_{40}Co_{60}$

Fig. 4 shows the field dependence of the resistivity for the $Ni_{75}Co_{25}$ alloy at 300 K for the LMR and TMR measurement configurations as measured up to $H = 70$ kOe, in qualitative agreement with the well-known room-temperature MR(H) curves reported for pure Ni metal [3,8,10]. The MR(H) curves for the $Ni_{40}Co_{60}$ alloy were very similar. The low-field sections of the measured magnetoresistance curves (not shown) with a hysteresis were qualitatively the same as at low temperature for both alloys.

It can be seen furthermore from Fig. 4 that in the saturated (monodomain) state at sufficiently high magnetic fields, the field dependence of the MR(H) curves is very similar for the LMR and TMR components, both indicating a nearly linear decrease of the resistivity above the saturation field.

The decrease of the resistivity with increasing magnetic field in the saturation region is due to the gradual suppression of the thermally-induced spin disorder [4,10,20–22] since at finite temperatures the scattering of conduction electrons on non-aligned individual magnetic moments also gives a contribution to the resistivity. By increasing the magnetic field after technical saturation (in the monodomain state), the thermally disordered magnetic moments are more and more aligned along the magnetic field [4] (this is often termed also as paraprocess [20]) and, therefore, this kind of scattering is diminished and, thus, one can observe a resistivity decrease.

We have displayed the data for the magnetic field range $|H| \geq 5$ kOe on a ρ(B) vs B plot by taking into account that $B = H + 4\pi M_s$ where $4\pi M_s(300K) = 8.965$ kG for the $Ni_{75}Co_{25}$ alloy and $4\pi M_s(300K) = 12.99$ kG for the $Ni_{40}Co_{60}$ alloy. A second-order polynomial fit provided a sufficiently accurate description of the experimental data for both alloys, the fit quality (R^2) being between 0.995 and 0.999 for the various datasets. The $\rho(B = 0)$ values were allowed again as free parameters.

By using the $\rho_L(B = 0)$ and $\rho_T(B = 0)$ data obtained above, we have displayed the room-temperature MR(H) data of the two Ni-Co alloys for $|H| \geq 5$ kOe on a Kohler plot in Fig. 5. A second-order polynomial was found to be satisfactory for a sufficiently accurate fitting of the data. The fit quality could not be improved by refining the $\rho_L(B = 0)$ and $\rho_T(B = 0)$ data.

Table 2
The same magnetoresistance parameters for the two Ni-Co alloys at $T = 300$ K which were shown for $T = 3$ K in Table I.

$T = 300$ K fitted parameters		$\rho(B = 0)$ (μΩ·cm)	α (μΩ·cm/kG)	β (μΩ·cm/(kG)^2)	ρ_{is} (μΩ·cm)	AMR parameters $\Delta\rho_{AMR}$ (μΩ·cm)	AMR ratio (%)
$Ni_{75}Co_{25}$ (#B3)	LMR	11.17	$-2.24{\cdot}10^{-3}$	$+3.94{\cdot}10^{-6}$	10.69	0.725	6.78
	TMR	10.45	$-2.63{\cdot}10^{-3}$	$+6.49{\cdot}10^{-6}$			
$Ni_{40}Co_{60}$ (#B4)	LMR	8.80	$-1.31{\cdot}10^{-3}$	$+3.69{\cdot}10^{-6}$	8.49	0.46	5.42
	TMR	8.34	$-1.50{\cdot}10^{-3}$	$+5.20{\cdot}10^{-6}$			

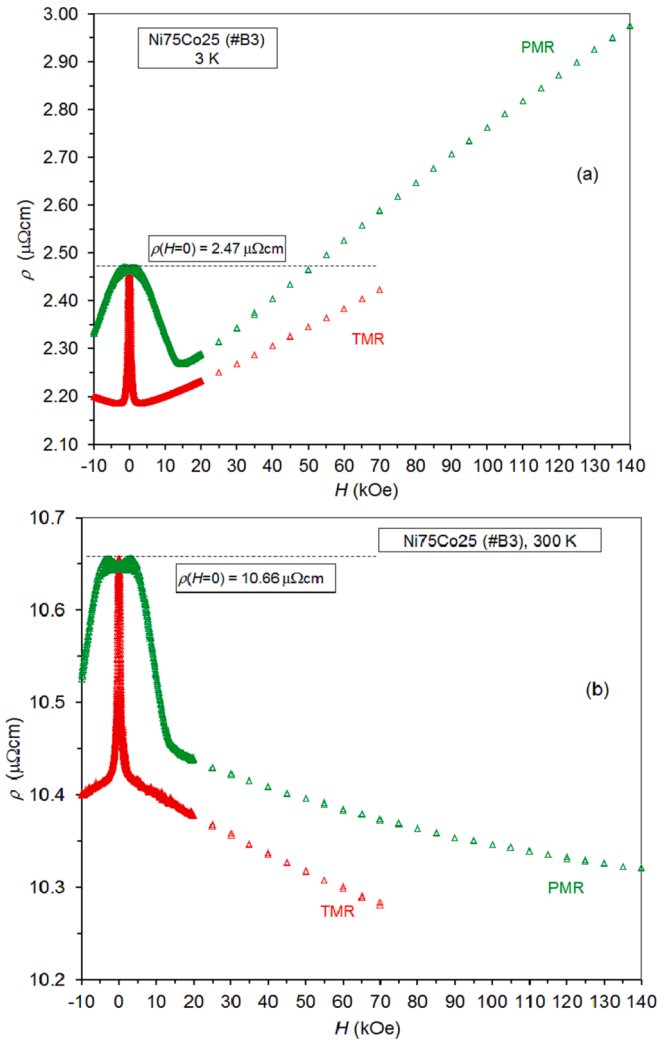

Fig. 7. Field dependence of the resistivity ρ at (a) $T = 3$ K and (b) $T = 300$ K for the $Ni_{75}Co_{25}$ alloy with magnetic field orientations as indicated (TMR, PMR) in the magnetic field range from −10 kOe to + 140 kOe.

Table A1
Parameters describing the functional form of the Kohler function $F(x)$ of the $Ni_{75}Co_{25}$ and $Ni_{40}Co_{60}$ alloys at $T = 3$ K and 300 K for the LMR and TMR configurations. The parameter values were obtained by fitting the experimental $\rho(B)/\rho(B = 0)$ vs $B/\rho(B = 0)$ data (Kohler plot) to the expression $1 + F[B/\rho(B = 0)]$ with the empirical function $F(x) = a\,x + b\,x^2$. The fit quality was $R^2 > 0.999$ ($T = 3$ K) and $R^2 > 0.99$ ($T = 300$ K).

$T = 3$ K fitted parameters		$\rho(B = 0)$ (μΩ·cm)	a (μΩ·cm/kG)	b (μΩ·cm/(kG)^2)
$Ni_{75}Co_{25}$ (#B3)	LMR	2.91	$+1.395\cdot10^{-3}$	$+30.44\cdot10^{-6}$
	TMR	2.14	$+2.844\cdot10^{-3}$	$+19.79\cdot10^{-6}$
$Ni_{40}Co_{60}$ (#B4)	LMR	1.95	$+3.903\cdot10^{-3}$	$+7.274\cdot10^{-6}$
	TMR	1.57	$+4.189\cdot10^{-3}$	$+5.049\cdot10^{-6}$
$T = 300$ K fitted parameters		$\rho(B = 0)$(μΩ·cm)	a(μΩ·cm/kG)	b (μΩ·cm/(kG)^2)
$Ni_{75}Co_{25}$ (#B3)	LMR	11.17	$-2.242\cdot10^{-3}$	$+44.08\cdot10^{-6}$
	TMR	10.45	$-2.634\cdot10^{-3}$	$+67.84\cdot10^{-6}$
$Ni_{40}Co_{60}$ (#B4)	LMR	8.80	$-1.332\cdot10^{-3}$	$+32.94\cdot10^{-6}$
	TMR	8.34	$-1.512\cdot10^{-3}$	$+43.63\cdot10^{-6}$

For visualizing better the qualitatively similar behavior of the field dependence of the resistivity and the quantitative differences for the two Ni-Co alloys, the magnetic-field-induced resistivity change $\Delta\rho(B) = \rho(B) - \rho(B = 0) = \alpha{\cdot}B + \beta{\cdot}B^2$ is displayed in Fig. 6 as a function of the magnetic induction B for both samples. The values of the parameters α and β as well as the $\rho(B = 0)$ values are collected in Table 2. together with the derived AMR parameters. The AMR ratio at $T = 300$ K matches well the reported room-temperature values [15] for both Ni-Co alloys.

The magnitude of the resistivity decrease is comparable with the result obtained previously on a nc-Ni sample [10] which is indicated by the solid thick red line in Fig. 6 for the TMR component. As observed and explained in the previous study [10] for both the microcrystalline and nanocrystalline Ni samples, the resistivity decrease at $T = 300$ K is stronger for the TMR component than for the LMR component also for the Ni-Co alloys, i.e., the relation $|\Delta\rho(\text{TMR})| > |\Delta\rho(\text{LMR})|$ holds both for pure Ni [10] and for the Ni–Co alloys.

In Ref. 10, the various theoretical approaches for describing the field dependence of the resistivity in the magnetically saturated state at high temperatures were discussed at some length. It was pointed out there that the derived theoretical formulae [20–22] do not properly account for the experimentally observed field dependence, which could be fairly accurately described empirically by a second-order polynomial function for pure Ni metal in both microstructural states. It was shown in the present work that the same is valid for the experimental data of the $Ni_{75}Co_{25}$ and $Ni_{40}Co_{60}$ alloys. This further emphasizes the need for a proper theoretical description of the resistivity decrease due to the magnon suppression process by an increasing external magnetic field. The available data also indicate that apparently the suppression of the magnons by high magnetic fields exerts a stronger influence on the transverse spin fluctuations than for the longitudinal ones. It is another challenge for the theory to account for the observed relation $|\Delta\rho(\text{TMR})| > |\Delta\rho(\text{LMR})|$.

5. Magnetoresistance properties with out-of-plane magnetic fields for the $Ni_{75}Co_{25}$ alloy (polar magnetoresistance, PMR)

Since in both the transverse (TMR) and polar (PMR) configurations the current flow is in the plane of the foil strip, and the magnetic field is in both cases perpendicular to the measuring current (TMR: in-plane (IP) magnetic field; PMR: out-of-plane (OP) magnetic field), it is reasonable to present the PMR(H) data in comparison with the TMR(H) data.

Fig. 7 shows the field dependence of the resistivity for the $Ni_{75}Co_{25}$ alloy in the PMR and TMR configurations at both $T = 3$ K and $T = 300$ K. The overall behavior of the PMR(H) curves is rather similar to the corresponding TMR(H) curves at both temperatures which were already discussed in Sections 3 and 4. The major difference between the PMR(H) and TMR(H) curves is in the saturation field (H_s) approximately marked by the break in the field evolution of the resistivity. The MR(H) curves in Fig. 7 reveal that the saturation field is about $H_{Ts} = 3$ kOe for the TMR (H) data whereas H_{Ps} in the PMR configuration is nearly 5 times higher for both temperatures. This is because H_{Ts} is determined by the in-plane magnetic anisotropy which may be just of the order of the observed saturation field for a polycrystalline sample of a $Ni_{75}Co_{25}$ alloy. On the other hand, the H_{Ps} value is mainly determined by the demagnetizing field H_d [12] which is $4\pi M_s = 9.35$ kOe at 3 K and 8.965 kOe at 300 K for a thin foil sample of this alloy in a direction perpendicular to the foil plane. The demagnetizing field corresponds actually to a shape anisotropy with a magnetic anisotropy field of $4\pi M_s$ in the foil plane. We should add to this value also the already noticed magnetic anisotropy in the foil plane as represented roughly by the H_{Ts} value. These two values sum up then to about 12.5 kOe which is already fairly close to the breaks in the PMR(H) curves in Fig. 7. As we could see above, the value of the saturation magnetization changes only slightly between 3 K and 300 K and the same holds true also for the eventual magnetocrystalline anisotropies and this explains that the breaks in the PMR(H) and TMR(H) curves appear approximately at the same magnetic fields at both

Table A2
Parameters describing the functional form of the Kohler function $F(x)$ of the microcrystalline (mc) and nanocrystalline (nc) Ni samples investigated in Ref. 10 at $T = 3$ K and 300 K for the LMR and TMR configurations. The parameter values were obtained by fitting the experimental $\rho(B)/\rho(B = 0)$ vs $B/\rho(B = 0)$ data (Kohler plot) to the expression $1 + F[B/\rho(B = 0)]$ with the empirical function $F(x) = a\,x + b\,x^2 + c\,x^3 + d\,x^4$ at $T = 3$ K and $F(x) = a\,x + b\,x^2$ at $T = 300$ K. The fit quality was $R^2 > 0.99$ for both $T = 3$ K and 300 K).

$T = 3$ K fitted parameters		$\rho(B = 0)$ (μΩ·cm)	a (μΩ·cm/kG)	b (μΩ·cm/(kG)^2)	c (μΩ·cm/(kG)^3)	d (μΩ·cm/(kG)^4)
mc-Ni (#B5)	LMR	0.01918	$+0.5875{\cdot}10^{-3}$	$-0.2589{\cdot}10^{-6}$	$+6.137{\cdot}10^{-11}$	$-5.711{\cdot}10^{-15}$
	TMR	0.01896	$+0.8358{\cdot}10^{-3}$	$-0.2718{\cdot}10^{-6}$	$+5.981{\cdot}10^{-11}$	$-5.385{\cdot}10^{-15}$
nc-Ni (#B2)	LMR	0.9797	$+0.0897{\cdot}10^{-3}$	$+4.064{\cdot}10^{-6}$	$-1.051{\cdot}10^{-8}$	0
	TMR	0.9640	$+0.2012{\cdot}10^{-3}$	$+4.830{\cdot}10^{-6}$	$-1.270{\cdot}10^{-8}$	0

$T = 300$ K fitted parameters		$\rho(B = 0)$ (μΩ·cm)	a(μΩ·cm/kG)	b(μΩ·cm/(kG)^2)
mc-Ni (#B5)	LMR	7.490	$-1.481{\cdot}10^{-3}$	$+18.64{\cdot}10^{-6}$
	TMR	7.318	$-1.543{\cdot}10^{-3}$	$+17.23{\cdot}10^{-6}$
nc-Ni (#B2)	LMR	8.893	$-1.345{\cdot}10^{-3}$	$+10.65{\cdot}10^{-6}$
	TMR	8.725	$-1.550{\cdot}10^{-3}$	$+1.862{\cdot}10^{-6}$

temperatures.

In support of the above considerations about the H_{Ps} value, we mention the results of Rijks et al. [23] who measured the PMR(H) curve for a 30 nm Permalloy ($Ni_{80}Fe_{20}$) film at $T = 5$ K. The resistivity reached saturation in the polar magnetic field at about $H_{Ps} = 10$ kOe which agrees very well with the standard value $4\pi M_s = 10$ kOe of Permalloy representing the demagnetizing field H_d. The good agreement of the saturation field and the demagnetizing field occurred in Ref. 23 because the in-plane magnetic anisotropy field of the Permalloy film was by three orders of magnitude smaller than the H_{Ps} value as indicated by the saturation field of the in-plane TMR(H) curve which was about 7 Oe only.

By noting that for the PMR configuration we have $B = H + 4\pi M_s - H_d = H$ [12], first we determined the $\rho_P(B = 0)$ value from the experimental $\rho_P(B)$ vs B data for both temperatures and the obtained values agreed with the $\rho_T(B = 0)$ data within less than 0.5 %. The same $\rho_P(B = 0)$ value was the optimum also from the Kohler plot of the PMR(H) data.

Since the magnetic field is perpendicular to the measuring current in both the TMR and PMR configurations, we can define two AMR ratios. An in-plane AMR ratio (AMR_{IP}) is defined by using the $\rho_L(B = 0)$ and $\rho_T(B = 0)$ values (and, likewise, an in-plane resistivity anisotropy splitting $\Delta\rho(AMR_{IP})$); these data have already been provided in Table 1 for $T = 3$ K and in Table 2 for $T = 300$ K. An out-of-plane AMR ratio (AMR_{OP}) is defined by using the $\rho_L(B = 0)$ and $\rho_P(B = 0)$ values (and, likewise, an out-of-plane resistivity anisotropy splitting $\Delta\rho(AMR_{OP})$). These derived out-of-plane parameters were as follows: $AMR_{OP} = 31.4$ % and $\Delta\rho(AMR_{OP}) = 0.754$ μΩ·cm for $T = 3$ K and $AMR_{OP} = 6.59$ % and $\Delta\rho(AMR_{OP}) = 0.705$ μΩ·cm for $T = 300$ K. The isotropic resistivity from the LMR and PMR was obtained as $\rho_{is} = 2.4$ μΩ·cm for $T = 3$ K and $\rho_{is} = 10.7$ μΩ·cm for $T = 300$ K. A comparison with the in-plane AMR parameters in the Table 1 and Table 2 reveals that the magnitude of the AMR_{IP} and AMR_{OP} ratios agree within 2 % at 3 K and 3 % at 300 K. The same holds true also for the $\Delta\rho(AMR_{IP})$ and $\Delta\rho(AMR_{OP})$ values. The agreement of the ρ_{is} values for the two cases is within 0.1 %.

For a polycrystalline macroscopic (bulk) foil-shaped sample, the magnetoresistance should be the same if the magnetic field is oriented in any direction in a plane perpendicular to the current flow direction. As a consequence, an agreement of the AMR parameters for the IP and OP configurations is expected for the $Ni_{75}Co_{25}$ alloy foil. This is because the investigated strip-shaped foil (with its physical dimensions of 5 mm x 1 mm x 55 μm) of the $Ni_{75}Co_{25}$ alloy can be considered as a macroscopic sample. Therefore, the close agreement of the AMR parameters for the two configurations corresponds to expectation.

It should be noted that previous semiclassical calculations of the AMR ratio [24] predicted a dimensionality effect for thin ferromagnetic films in that both the AMR_{IP} and AMR_{OP} ratios decreased drastically when reducing the film thickness down to below about 1 μm. This decrease was ascribed to the contribution of surface scattering effects to the resistivity (it follows that these scattering events, at the same time, do not contribute effectively to the resistivity anisotropy splitting, i.e., this results then in a decrease of the AMR ratio). It turned out, furthermore, that in the thickness range where the surface scattering already reduces the AMR ratio, the AMR_{OP} ratio is typically by about a factor of 1.5 larger than the AMR_{IP} ratio. In the thick-film (bulk) limit, the two AMR ratios were obtained as equal. Later, Rijks et al. [23] performed experiments to measure the AMR_{IP} and AMR_{OP} ratio for thin Permalloy ($Ni_{80}Fe_{20}$) films with thicknesses from 5 to 100 nm at $T = 5$ K. The experiments confirmed both the reduction of the AMR ratio below about 100 nm and the higher values of the AMR_{OP} ratio by roughly the theoretically predicted factor in this thickness range. Since our $Ni_{75}Co_{25}$ alloy foil sample had a thickness of 55 μm, the above-described dimensionality effect does not occur and, thus, the AMR_{IP} and AMR_{OP} ratios should show a good agreement with each other as was actually observed.

6. Summary

In the present work, the field dependence of the resistivity of $Ni_{75}Co_{25}$ and $Ni_{40}Co_{60}$ bulk alloys was measured at $T = 3$ K and 300 K up to high magnetic fields. In addition to the determination of the AMR ratio, the accuracy of the present data enabled also to make important statements about the field dependence of the resistivity.

The main interest in the present paper was in the AMR parameters which could be derived from the resistivity in the magnetically saturated (monodomain) state achieved in high magnetic field. The measured resistivity vs magnetic field data could be well fitted to an empirical second-order polynomial function for these alloys at both temperatures. For the determination of the AMR parameters, the required zero-induction resistivity values were extracted from the experimental data by the Kohler analysis.

The values of the AMR ratio for the two Ni-Co alloys were found to be close to the relevant previous data both at low and high temperatures [15]. An important point is, however, that due to the measurement precision and careful data evaluation, our AMR data obtained on well-characterized samples can be considered as reference values for the bulk state of the investigated compositions.

A few important points emerging from the present work can be listed as follows.

i. By determining the resistivity of the alloy samples, we could report not only the AMR ratios, but also the resistivity anisotropy splitting $\Delta\rho_{AMR}$ which is of importance for comparison with theoretical calculations.
ii. The precision of the data enabled the determination of an empirical functional form of the field dependence of the resistivity in the magnetically saturated region, i.e., in the single-domain state both at $T = 3$ K and $T = 300$ K.
iii. The empirically established field dependence of the resistivity in the magnetically saturated (single-domain) state at $T = 3$ K was found to contain, in addition to the usual quadratic term due to the OMR effect, also a linear term for both alloys as reported also for pure Ni in a previous work [10]. Further theoretical work is required to establish if the true description of the OMR effect should either contain a linear term as well or the latter term has a different origin.
iv. The present results for the resistivity at $T = 300$ K revealed for both alloys that the field dependence of the resistivity in the magnetically saturated (single-domain) state can be described empirically to a high accuracy with the sum of a linear and a quadratic term as found also for pure Ni in a previous work [10]. As discussed in detail in Ref. 10, the available theoretical descriptions yielded a different functional form for the field dependence of the resistivity around this temperature. Therefore, a refinement of the theoretical description of the field dependence of the resistivity decrease due to the magnon suppression process is required.
v. The precision of the present data also enabled the empirical determination of the Kohler function F the form of which cannot be derived theoretically. It turned out that the Kohler function F has the functional form $F(x) = a\,x^2 + b\,x$ for these Ni-Co alloys at both $T = 3$ K and 300 K (parameters a and b are summarized in the Appendix, see Table A1.). In a previous work [10], the same functional form was obtained at $T = 300$ K for both a nanocrystalline and a microcrystalline (bulk) Ni sample whereas at $T = 3$ K the functional form was a fourth-order polynomial for bulk Ni and a third-order polynomial for nanocrystalline Ni. The higher-order polynomial forms may be a consequence of the much lower resistivity of the pure Ni sample in either of the two microstructural modifications which result in much longer electron mean free path values leading to a stronger ordinary magnetoresistance contribution.
vi. The results of the present work on two Ni-Co alloys and those of a previous work on pure Ni [10] indicate that if the zero-field resistivity of a metallic ferromagnet is at least as high as about 1 μΩcm, the extrapolation of the $\rho(B)$ data to $B = 0$ even at low temperatures yields to a high accuracy the same zero-induction resistivity, which is needed for the correct AMR ratio determination, as that derived from an exact analysis based on the Kohler plot evaluation. Furthermore, if the zero-field resistivity is well above this critical value, which is usually the case for concentrated alloys at any temperature or for pure ferromagnetic metals at elevated temperatures such as 300 K or higher, then even a $\rho(H \rightarrow 0)$ extrapolation usually yields a resistivity value which agrees well with the value of the $\rho(B \rightarrow 0)$ extrapolation within the experimental uncertainty of the measurement. Below the critical zero-field resistivity, however, the use of the Kohler plot for getting the correct $\rho(B = 0)$ value is unavoidable due to the high uncertainty of the extrapolation to $B = 0$ in these cases.

Author declaration

Herewith we declare that the work described has neither been published nor is under consideration for publication elsewhere and that its publication is approved by all authors.

CRediT authorship contribution statement

I. Bakonyi: Writing – review & editing, Writing – original draft, Funding acquisition, Formal analysis, Conceptualization. **F.D. Czeschka:** Investigation, Formal analysis, Data curation. **V.A. Isnaini:** Investigation, Data curation. **A.T. Krupp:** Investigation, Data curation. **J. Gubicza:** Writing – review & editing, Investigation, Data curation. **L. K. Varga:** Resources, Methodology. **L. Péter:** Writing – review & editing, Investigation, Data curation.

Declaration of competing interest

The authors declare that they have no known competing financial interests or personal relationships that could have appeared to influence the work reported in this paper.

Data availability

Data will be made available on request.

Acknowledgements

The HUN-REN Wigner Research Centre for Physics utilizes the research infrastructure of the Hungarian Academy of Sciences (HAS). The authors acknowledge the support of the DFG within the priority program SPP 1666. One of the authors (I.B.) is indebted to the Alexander von Humboldt Foundation, Germany for a one-month fellowship and to H. Ebert (Ludwig-Maximilians-Universität, München) for the kind hospitality during this research stay as well as for useful comments on the manuscript. The authors also acknowledge S.T.B. Gönnenwein and R. Gross (Walther-Meissner Institute for Low Temperature Research, Bavarian Academy of Sciences and Humanities, Garching) for generously putting the necessary experimental facility at our disposal in their laboratory for carrying out the resistivity measurements described here. We are indebted to the Eötvös Loránd University, Budapest, Hungary for providing a PhD fellowship to V.A.I. via a Stipendium Hungaricum scholarship. The authors appreciate the discussions and comments by L. F. Kiss on the revised manuscript.

Data availability statement: The data that support the findings of this study are available from the author upon reasonable request.

Appendix

As discussed in Section 3, the dependence of the resistivity of a metallic ferromagnet on magnetic induction is expected to obey Kohler's rule which can be transformed into the form $\rho(B)/\rho(B = 0) = 1 + F[B/\rho(B = 0)]$ where F is the Kohler function. When displaying the experimental data in the form $\rho(B)/\rho(B = 0)$ vs $B/\rho(B = 0)$, we get a so-called Kohler plot from which the function F can be determined empirically by fitting the data to a chosen function. It turned out in the present work that for the present two Ni-Co alloys the data can be fitted at both temperatures with high accuracy to an empirical second-order polynomial function, i.e., the Kohler function F has the functional form $F(x) = a\,x + b\,x^2$. The fit parameters of the Kohler function are summarized in Table A1. for the present Ni-Co alloys. For comparison, the fit parameters for the recently studied bulk and nc Ni samples [10] are given in Table A2..

References

[1] A. Hirohata, K. Yamada, Y. Nakatani, I.L. Prejbeanu, B. Diény, P. Pirro, B. Hillebrands, J. Magn. Magn. Mater. 509 (2020) 166711.
[2] J.M. Daughton, J. Magn. Magn. Mater. 192 (1999) 334.
[3] R.M. Bozorth, Ferromagnetism, Van Nostrand, New York, 1951.
[4] T.R. McGuire, R.I. Potter, IEEE Trans. Magn. 11 (1975) 1018.

[5] I.A. Campbell and A. Fert, *Transport Properties of Ferromagnets*. In: Ferromagnetic Materials, Vol. 3, Ch. 9, ed. E.P. Wohlfarth (North-Holland, Amsterdam, 1982). https://doi.org/10.1016/S1574-9304(05)80095-1.
[6] R.C. O'Handley, Modern Magnetic Materials, Principles and Applications (Wiley-Interscience, New York, 2000.
[7] L. Nádvorník, M. Borchert, L. Brandt, R. Schlitz, K.A. de Mare, K. Výborný, I. Mertig, G. Jakob, M. Kläui, S.T.B. Goennenwein, M. Wolf, G. Woltersdorf, T. Kampfrath, Phys. Rev. X 11 (2021) 021030.
[8] V.A. Isnaini, T. Kolonits, Z. Czigány, J. Gubicza, S. Zsurzsa, L.K. Varga, E. Tóth-Kádár, L. Pogány, L. Péter, I. Bakonyi, Eur. Phys. J. plus 135 (2020) 39.
[9] M. El-Tahawy, L. Péter, L.F. Kiss, J. Gubicza, Zs. Czigány, G. Molnár, I. Bakonyi, J. Magn. Magn. Mater. 560 (2022) 169660.
[10] I. Bakonyi, F.D. Czeschka, L.F. Kiss, V.A. Isnaini, A.T. Krupp, K. Palotás, S. Zsurzsa, L. Péter, Eur. Phys. J. plus 137 (2022) 871.
[11] M. Kohler, Ann. Phys. 32 (1938) 211.
[12] I. Bakonyi, Eur. Phys. J. plus 133 (2018) 521.
[13] J.M. Ziman, Electrons and Phonons, Clarendon Press, Oxford, 1960, p. 490.
[14] F.C. Schwerer, J. Silcox, J. Appl. Phys. 39 (1968) 2047.
[15] B.G. Tóth, L. Péter, Á. Révész, J. Pádár, I. Bakonyi, Eur. Phys. J. B 75 (2010) 167.
[16] J. Gubicza. X-ray Line Profile Analysis in Materials Science, IGI-Global, Hershey, PA, USA, 2014, ISBN 978-1-4666-5852-3 (igi-global.com).
[17] I. Bakonyi, V.A. Isnaini, T. Kolonits, Zs. Czigány, J. Gubicza, L.K. Varga, E. Tóth-Kádár, L. Pogány, L. Péter, H. Ebert, The specific grain-boundary electrical resistivity of Ni, Philos. Magaz. 99 (2019) 1139.
[18] C. Kittel, Introduction to Solid State Physics, 6th edition, Wiley, New York, 1986.
[19] D. Gall, J. Appl. Phys. 119 (2016) 085101.
[20] B. Raquet, M. Viret, J.M. Broto, E. Sondergard, O. Cespedes, R. Mamy, J. Appl. Phys. 91 (2002) 8129.
[21] B. Raquet, M. Viret, E. Sondergard, O. Cespedes, R. Mamy, Phys. Rev. B 66 (2002) 024433.
[22] P.V.P. Madduri, S.N. Kaul, Phys. Rev. B 95 (2017) 184402.
[23] T.G.S.M. Rijks, S.K.J. Lenczowski, R. Coehoorn, W.J.M. de Jonge, Phys. Rev. B 56 (1997) 362.
[24] T.G.S.M. Rijks, R. Coehoorn, M.J.M. de Jong, W.J.M. de Jonge, Phys. Rev. B 51 (1995) 283.